NOTE

Using dynamical mode decomposition to extract the limit cycle dynamics of modulated turbulence in a plasma simulation

IOP ebooks™

Bringing you innovative digital publishing with leading voices to create your essential collection of books in STEM research.

Start exploring the collection - download the first chapter of every title for free.

Note

Using dynamical mode decomposition to extract the limit cycle dynamics of modulated turbulence in a plasma simulation

M Sasaki[1,2,3] , **Y Kawachi**[4]**, R O Dendy**[2,3,5]**, H Arakawa**[6] **, N Kasuya**[1,2]**,
F Kin**[7]**, K Yamasaki**[1] **and S Inagaki**[1,2]

[1] Research Institute for Applied Mechanics, Kyushu University, Kasuga 816-8580, Japan
[2] Research Center for Plasma Turbulence, Kyushu University, Kasuga 816-8580, Japan
[3] Centre for Fusion, Space and Astrophysics, Department of Physics, Warwick University, Coventry CV4 7AL, United Kingdom
[4] Interdisciplinary Graduate School of Engineering Sciences, Kyushu University, Kasuga 816-8580, Japan
[5] CCFE, Culham Science Centre, Abingdon, Oxfordshire OX14 3DB, United Kingdom
[6] Institute of Science and Engineering, Academic Assembly, Shimane University, Matsue 690-8504, Japan
[7] National Institutes for Quantum and Radiological Science and Technology, Naka 311-0193, Japan

E-mail: sasaki@riam.kyushu-u.ac.jp

Abstract
The novel technique of dynamical mode decomposition (DMD) is applied to the outputs of a numerical simulation of Kelvin–Helmholtz turbulence in a cylindical plasma, so as to capture and quantify the time evolution of the dominant nonlinear structures. Empirically, these structures comprise rotationally symmetric deformations together with spiral patterns, and they are found to be identified as the main modes of the DMD. A new method to calculate the time evolution of DMD mode amplitudes is proposed, based on convolution-type correlation integrals, and then applied to the simulation outputs in a limit cycle regime. The resulting time traces capture the essential physics far better than Fourier techniques applied to the same data.

Keywords: dynamical mode decomposition, turbulence imaging, Kelvin–Helmholtz instability, limit cycle oscillation

(Some figures may appear in colour only in the online journal)

1. Introduction

Strongly nonlinear phenomena are ubiquitous in plasma physics, both in experimental measurements and in the outputs from numerical simulations. The nonlinear phenomenology may be temporally transient [1, 2] or sustained [3], spatially localised [4] or global [5]. Identifying the dominant dynamical features and their interactions, and quantifying their time evolution, is therefore a central task. Fourier decomposition has major limitations in this context, because the empirically identified key structures are localised with a finite extent, and therefore require a very large number of Fourier modes to represent them.

Here we consider the application of dynamical mode decomposition (DMD) [6–8] to this problem. DMD is attractive, in that it: assumes no functional form for the structures; is entirely data-driven, see equation (1) below; and is mathematically linear—mode identification and growth rates reduce to an eigenvector-eigenvalue procedure. When the time evolution of the mode amplitude is modulated, as in most cases of turbulence, the single DMD derived growth rate is insufficient to capture the dynamics. Here we therefore
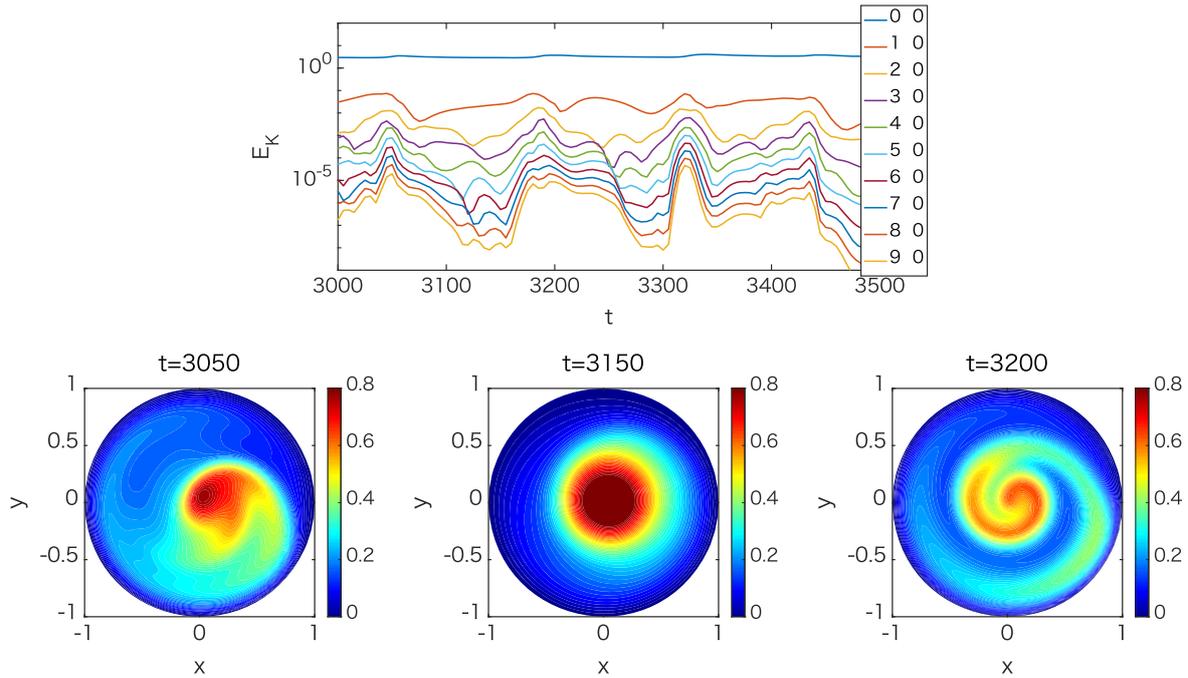
Figure 1. Top: Time evolution of the energy (logarithmic scale) in each cylindrical Fourier mode (m, n) of the simulation in its saturated phase, for integer $0 < m < 9$ and $n = 0$. Here m and n denote axial and azimuthal mode numbers. The background corresponds to the mode $(0, 0)$. Quasiperiodic energy flows are evident, and the flow into higher m-numbers indicates the formation of sharper spatial gradients associated with nonlinear structures at those times. Bottom: Full two-dimensional spatial patterns of the density from the direct numerical simulation at $t = 3050$, 3150 and 3200.

propose and develop a method to extract the modulation dynamics from the outputs of the DMD technique, as applied to a simulation of turbulence in a cylindrical plasma.

2. Extraction of nonlinear dynamics

The turbulence dataset is obtained from a direct numerical simulation, based on an extension of the Hasega-Wakatani reduced fluid model which includes ion-neutral collisions and electron parallel velocity evolution [9, 10]. Turbulent and nonlinear phenomena can be simulated, such as those arising from resistive drift waves and the Kelvin–Helmholtz (KH) instability in linear devices [11, 12]. The turbulence addressed here originates from the KH instability for the plasma parameters in MISTRAL [12]. Its phenomenology includes a limit cycle oscillation between the background plasma and turbulent fluctuations; for more detail, see [13]. The time evolution of the energy of each Fourier mode in a saturated state, and the two-dimensional patterns of the density at $t = 3050$, 3150 and 3200, are shown in figure 1, where time t is normalized by the ion gyrofrequency. The energies (squared amplitudes) of the background and the turbulence are modulated in time: the period of the limit cycle, $T_{LCO} \sim 100$, which is much longer than the timescale of turbulent oscillation, $T_{turb} = O(10)$. The computational time-step is much smaller, $\delta t = 2 \times 10^{-2}$. The spatial pattern in figure 1 changes on the timescale T_{LCO}. Let us now apply the DMD to the underlying dataset, and then propose and develop a novel method to extract the modulation dynamics.

We represent the system at time t by an array (state vector) $\mathbf{X} = \mathbf{X}(\mathbf{r}_1, \mathbf{r}_2, \cdots | t_1, t_2, \cdots)$, which is a matrix recording the value of the set of simulation outputs $\mathbf{X}$ (for example, density) at each point r_j and at each time t_j. The system transits to the state $\mathbf{X}' = \mathbf{X}(\mathbf{r}_1, \mathbf{r}_2, \cdots | t_1 + \Delta t, t_2 + \Delta t, \cdots)$, where δt is the unit of time resolution chosen for DMD analysis. Here $\delta t = 5$, which is large enough to reduce the computational cost, while remaining sufficient to resolve the turbulence evolution. In the DMD approach, we focus on the properties of the matrix A which generates the mapping

$$\mathbf{X}' = A\mathbf{X}, \tag{1}$$

whereas $\mathbf{X}$ and $\mathbf{X}'$ comprise datasets, A is taken to embody the physical dynamics of, in the present case, Kelvin–Helmoltz plasma turbulence. The challenge is, first, to reduce the rank of A to manageable level using singular value decomposition (SVD) [14], and then to identify the dominant eigenvalues and eigenvectors of A. The eigenvectors Ψ are the DMD modes: they correspond to the dominant nonlinear spatial structures, and represent their action in the time evolution of the data. The details of the DMD approach are summarized in the appendix. In outline, mathematically

$$\Psi = \mathbf{X}' V_r \Sigma_r^{-1} \xi. \tag{2}$$

Here, the matrices V and Σ are obtained from the SVD of $\mathbf{X}$, and satisfy $\mathbf{X} = U\Sigma V^*$; U and V are unitary matrices, and Σ is the diagonal matrix consisting of the singular values of X. The subscript r indicates the matrix is truncated to the rank r. ξ is the eigenvector of $U_r^* A U_r$, which is the projection of A on U. In this way, the key structures, together with their
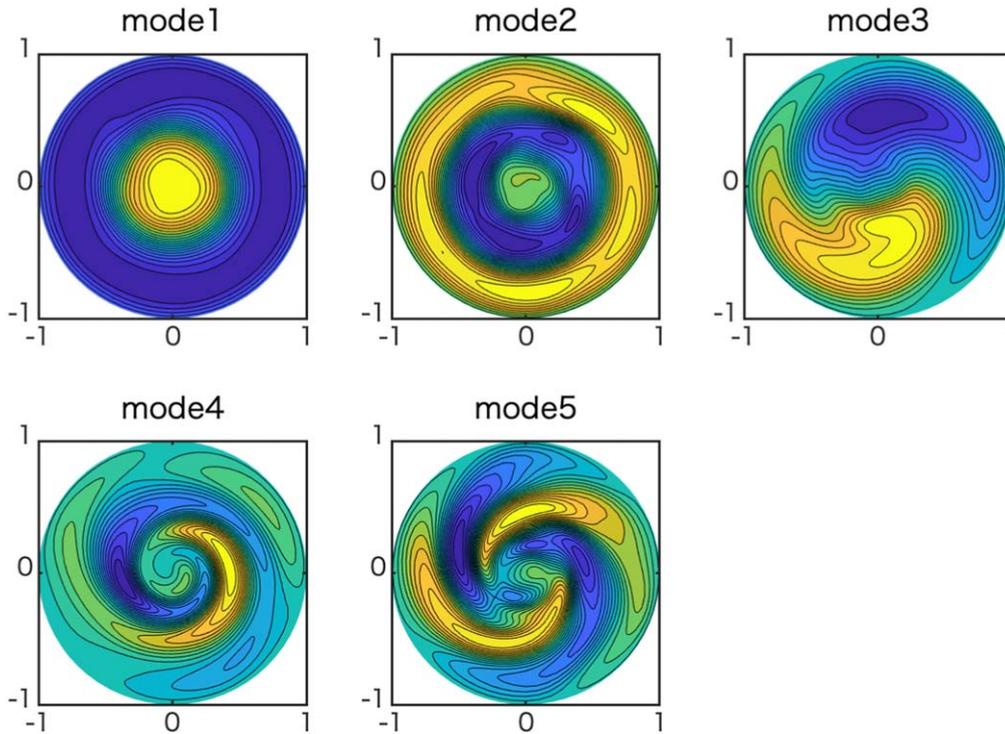
Figure 2. The five dominant eigenvectors, in the form of two-dimensional spatial patterns, derived from DMD analysis of the simulation outputs. These are the dominant nonlinear structures, Mode1 to Mode5, discussed in the main text.
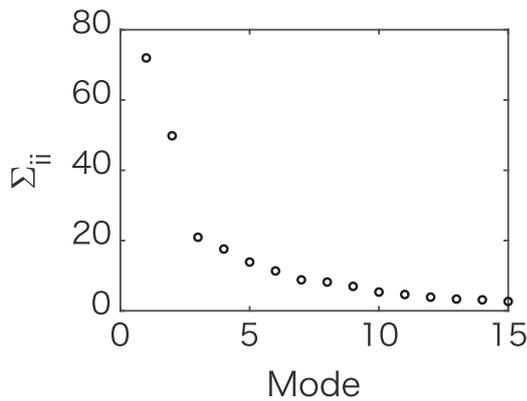
Figure 3. Singular values for each of the DMD modes, calculated from the diagonal component of the matrix Σ.

frequency and growth rate, are simultaneously obtained by DMD. This approach is model-independent and does not draw on knowledge of the underlying physical processes. The DMD eigenmodes are typically strongly nonlinear spatial structures, which would require numerous Fourier modes to represent them, see appendix B. Hence, the DMD approach greatly reduces the number of effective degrees of freedom, compared to a Fourier-based approach.

Figure 2 illustrates the leading DMD modes obtained for the density fluctuation $\tilde{n}(r, \theta, t)$ in the turbulence simulation. The singular value for each of the DMD modes, which represents the importance of the DMD mode for the dynamics of the system, is calculated from the diagonal component of the matrix Σ. These values are shown in figure 3, which motivates our truncation of the rank r of A at $r = 9$, for which

the singular value is a factor five below that of Mode1. These DMD modes show the characteristic spatial structures: Mode1 and Mode2 correspond to the deformation of the background; Mode3 is the dominant fluctuation pattern; and Mode4 and Mode5 are the spiral structures, which transiently appear and disappear on the timescale of the limit cycle oscillation [13]. All the physical structures rotate in the azimuthal direction, so that each eigenvector has a counterpart complex conjugate pattern. Together, they represent each rotating mode, and each mode in the pair has the same eigenvalue as its complex conjugate. The real and imaginary parts of the DMD eigenvalue define the frequency and growth rate, respectively, of the corresponding DMD mode. However, when the turbulence is modulated, as in the case of the limit cycle oscillation here, a single growth rate cannot express the temporal dynamics. Thus, we must now develop a method to extract how the amplitude of each DMD mode changes with time.

We first propose a method to define the magnitude of each DMD mode. By calculating the instantaneous correlation coefficient between each DMD mode and the full turbulence dataset, the dynamical change of the amplitudes of a DMD mode can be deduced. This correlation can be estimated from the convolution integral

$$F_j(r, \theta, t) = \frac{\int \tilde{n}(r - r', \theta - \theta', t)\hat{\Psi}_j(r', \theta')r'dr'd\theta'}{\int \tilde{n}(r', \theta', t)r'dr'd\theta'}. \quad (3)$$

Here $\hat{\Psi}_j$ is the jth DMD mode, normalized such that the two-dimensional spatial integral is unity. Recalling that the spatial pattern of the turbulence propagates in the azimuthal
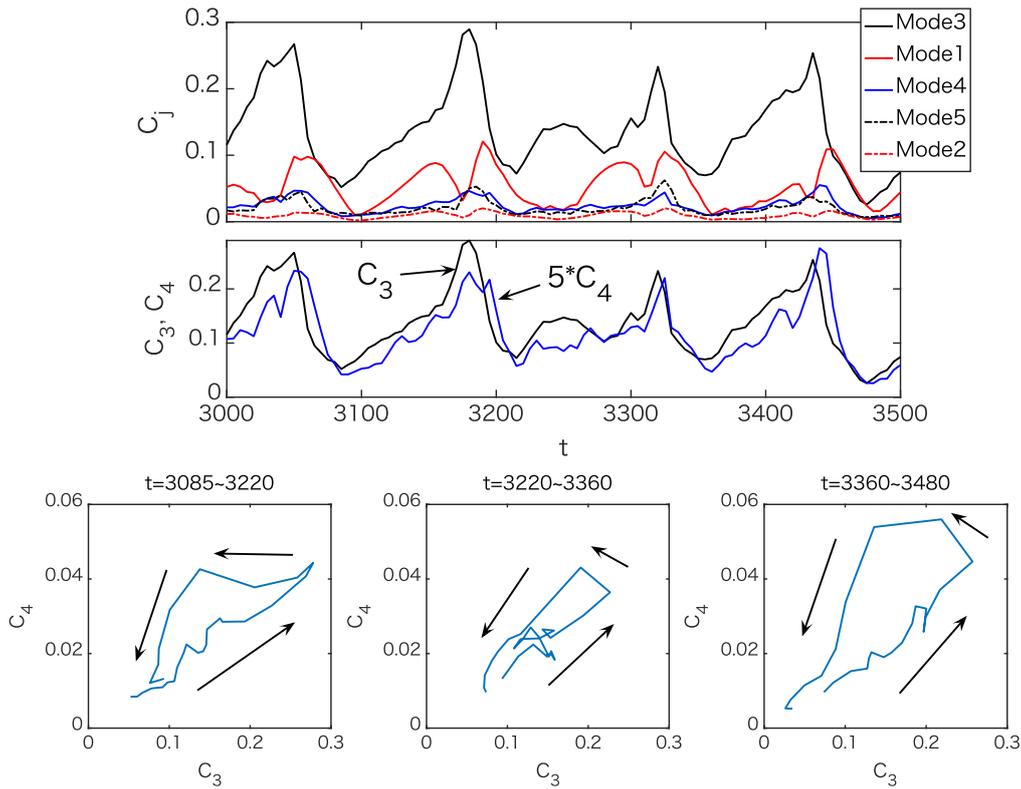
Figure 4. Top: Time evolution of the correlation coefficient C_j (see equations (3) and (4)), tracing the changing relative amplitude of the five DMD eigenvectors depicted in figure 2 in the simulation outputs. Middle: Time evolution of C_3 and $5 \times C_4$, re-plotted on the same scale to assist comparison. Bottom: Time evolution of the system plotted in the (C_3, C_4) plane, for three successive cycles identified from the upper panel. These closed Lissajous figures demonstrate the limit cycle dynamics that govern C_3 (KH instability) and C_4 (spiral structure) in combination.

direction, the correlation can be defined as

$$C_j(t) = \max [F_j(r, \theta, t)]. \qquad (4)$$

C_j defines an effective amplitude for each DMD mode. The calculated time evolution of C_j is plotted in figure 4 for Mode1 to Mode5. This captures the changing contribution of each structure to the overall turbulence. The limit cycle between the deformation of the background and the dominant turbulence, with the appearance and disappearance of the spiral structure [13], is immediately evident. Mode1 and Mode2, which correspond to the deformation of the background, show similar time evolution. The time evolution of Mode3 and Mode4, which correspond to the dominant turbulent fluctuation (KH instability) and spiral structure, respectively, precedes that of Mode1 and Mode2 by an interval $\delta t \approx 10$; this can be inferred from comparison of the upper and middle panels of figure 4. This implies a causal connection, which arises from how the turbulent fluctuation changes the background, which is discussed later in more detail. In order to see the relationship between the fluctuation patterns, the closed cycle Lissajous figures in the (C_3, C_4) plane are shown in the lower panel of figure 4, which clearly captures the causal relation between the KH instability and the spiral structure. They increase together, and then at a critical amplitude of the KH instability, the spiral structure becomes suddenly stronger, which leads to the suppression of the KH instability. Both amplitudes then decline to their

starting point. Thus, the growth in the amplitude of the KH instability is constrained, and eventually reversed, by the excitation of the spiral structure, which itself finally decays. The next circulation on this limit cycle then commences. The approach presented here, of combining the DMD method and the correlation integral, equation (3), enables one to create an approximation to the attractor for this strongly nonlinear and turbulent plasma system. We note that the correlation integral approach introduced here could also be used in the same way for the SVD [14–16] and proper orthogonal decomposition [17] methods. It is also potentially relevant to experimental imaging techniques such as those exploiting gas puffing [18–20], beam emission spectroscopy [21, 22], and visible light tomography [23, 24].

Finally, we turn to the physics of the system dynamics as inferred from the behaviour of the DMD modes. Mode3 corresponds to the KH instability, which is driven by the spatial gradient of the vorticity, $\partial_r^2 \langle V_\theta \rangle$, where $\langle V_\theta \rangle$ is the background azimuthal flow. The spiral structure (Mode4) has been identified as the instability which arises from the combination of the cylindrical effect and the flow inhomogeneity [13], which is different from the KH instability. Thus, two types of instability coexist in this system. The system dynamics can be understood by considering the time evolution of the fluctuations (Mode3 and Mode4) and of the background (Mode1) as follows. Figure 5 displays the evolution of; (a) these three normalized DMD modes; (b) the
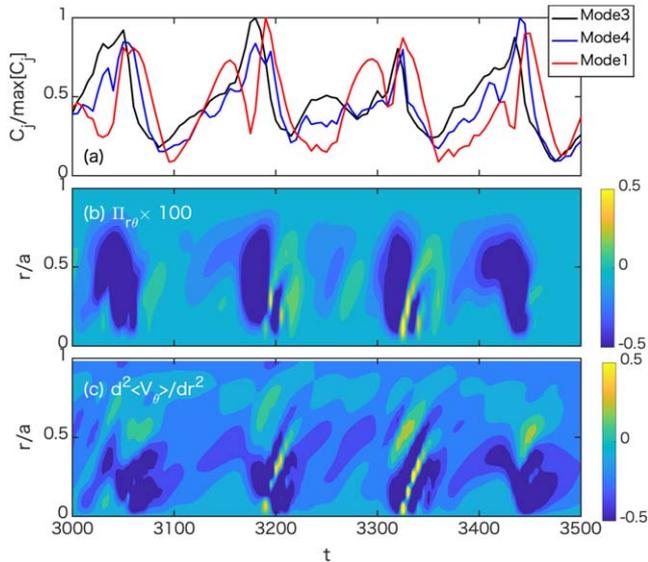
Figure 5. Time evolution of three DMD mode amplitudes, normalized to their peak values during $3000 < t < 3500$. Middle: Radial profiles of the fluctuation-induced momentum flux $\Pi_{r,\theta}$. Bottom: Radial profiles of background deformation, $\partial_r^2 \langle V_\theta \rangle$.

fluctuation-induced momentum flux $\Pi_{r,\theta}$ (for the definition, see equation (12) of [13]); and (c) the background flow. Here, each DMD mode amplitude is normalized by its maximum value attained between $t = 3000$ and $t = 3500$, to assist identifying time lags and causality. Figure 5 (top panel) shows that the peak level of the fluctuations (Mode3 and Mode4) precedes that of the background (Mode1) by an interval $\delta t \approx 10$. All three panels of figure 5 show that Mode3 induces a negative momentum flux which suppresses the vorticity gradient (driving source of KH), and that Mode4 induces a positive momentum flux which increases the vorticity gradient. Because the momentum flux $\Pi_{r,\theta}$ sensitively depends on the radial wavenumber, a structure with large k_r, such as the spiral structure, can drive the momentum flux effectively. Thus, although the amplitude of the spiral structure is not so large (as seen in the top panel of figure 4), the momentum flux driven by the spiral structure can be comparable to that driven by the KH instability. In this way, the KH instability and the spiral structure couple with each other through the background flow, and perform their different roles. The balance between the transport due to the each structure determines the dynamics of the limit cycle oscillation. Following the time evolution of the DMD modes clearly captures the contributions of the key structures to the dynamics of the system.

3. Conclusions

We have shown that the DMD technique, augmented by the correlation integral approach introduced in equations (3) and (4), has great potential for the quantitative characterization of turbulent and strongly nonlinear phenomenology in plasmas. Using this method, we have systematically extracted the time

evolution of the magnitude of each of the dominant, spatially coherent, global nonlinear structures (figure 4, upper), together with their coupled cyclic behaviour (figure 4, lower). This would not be extremely difficult using Fourier mode decomposition. The method introduced here remains valid, even when the amplitude of the structure changes drastically on a timescale much longer than the typical fluctuation period; whereas the conventional DMD method applies on shorter timescales, comparable to the turbulence period. Hence, by combining conventional DMD with the present method, turbulence phenomenology that is multi-timescale (from the turbulence timescale to the transport timescale) can be systematically addressed and quantified.

Appendix A. A brief summary of DMD

In the DMD method [6–8], the dynamical system is expressed as $\mathbf{X}(\mathbf{r}_1, \mathbf{r}_2, \cdots | t_1, t_2, \cdots)$, where r_j and t_j are the measurement location and time, respectively. So, if one observes the system with grids that span space with N elements and time with M elements, the size of the matrix A is $N \times M$. The DMD method assumes that the system can be described by the linear combination of nonlinear dynamical states, as in equation (1), where the operator A governs the system evolution. The operator A is determined entirely from the observable data, as

$$A = X'X^{\dagger}. \tag{A.1}$$

The size of X is usually so large that a reduction of the dataset is necessary. To achieve this, we use the SVD technique [14]. Formally, we write

$$\begin{aligned} X &= U\Sigma V^*, \\ &\approx U_r \Sigma_r V_r^*, \end{aligned} \tag{A.2}$$

where the subscript r denotes the r-rank truncation. Here, a general matrix is decomposed into two unitary matrices, U and V, which are combined with the diagonal matrix Σ, containing the singular values of the original matrix; $\Sigma_{ii} \neq 0$, $\Sigma_{ij} = 0$
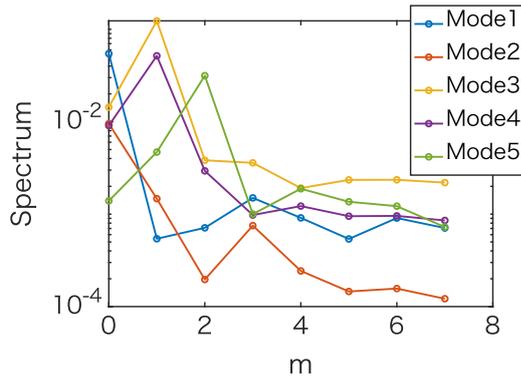
Figure B1. Amplitudes, plotted on a logarithmic scale, of the leading poloidal Fourier components of the five DMD eigenvectors displayed in figure 2, for azimuthal mode number m in the range $0 \leqslant m \leqslant 7$.

$(i \neq j)$ [14]. It is necessary to construct the matrix $\tilde{A}$, which is the projection of A onto U_r:

$$\begin{aligned} \tilde{A} &= U_r^* A U_r \\ &= U_r^* X' V_r \Sigma_r^{-1}. \end{aligned} \quad \text{(A.3)}$$

The eigenvalue problem for A is then recast as

$$\tilde{A}\xi = \Lambda\xi. \quad \text{(A.4)}$$

The eigenvalues Λ and eigenvectors ξ of $\tilde{A}$ are next obtained from equation (A.4). Because the eigenvalues of A and $\tilde{A}$ are the same, the eigenvector of A, Ψ, is given as

$$\Psi = U_r' \xi = X' V_r \Sigma_r^{-1} \xi. \quad \text{(A.5)}$$

The eigenvector Ψ is called the DMD mode. Finally, the time evolution of the system $x(t)$ is expressed by using DMD modes as

$$x(t) = \Psi e^{\Omega t} \Psi^\dagger x(0), \quad \text{(A.6)}$$

where $x(0)$ is the initial condition. We emphasize that this expression can be used only for the short timescale evolution, comparable to the fluctuation period, and given monotonic growth or damping. This is because the mode amplitude $\Psi^\dagger x(0)$ in equation (A.6) is constant in time. Quantifying the time evolution of the modulated turbulence, where the amplitude changes dynamically, is therefore difficult using DMD alone; hence the present paper.

Appendix B. Fourier decomposition of DMD eigenvectors

Figure B1 plots the amplitudes (on a logarithmic scale) of the leading azimuthal Fourier components of the five DMD eigenvectors displayed in figure 2. Here the Fourier expansion is with respect to basis eigenfunctions $\exp(im\theta)$, where θ is azimuthal angle and, in figure B1, m takes integer values in the range $0 \leqslant m \leqslant 7$. In order to show the spectrum simply, we have not attempted to calculate Fourier amplitudes for $m > 7$. Figure B1 shows that all DMD eigenvectors except Mode1 and Mode2 incorporate multiple Fourier components that contribute to form steep wavefronts in the azimuthal direction. In contrast, the DMD method can directly extract the key nonlinear structures, which simplifies the system dynamics.

ORCID iDs

M Sasaki ⓘ https://orcid.org/0000-0001-6835-1569
H Arakawa ⓘ https://orcid.org/0000-0001-9793-099X

References

[1] Connor J W 1998 *Plasma Phys. Control. Fusion* **40** 531
[2] Sarazin Y *et al* 1998 *Phys. Plasmas* **5** 4214
[3] Diamond P H *et al* 2005 *Plasma Phys. Control. Fusion* **47** R35
[4] Krasheninnikov S I *et al* 2017 *Nucl. Fusion* **57** 102010
[5] Wagner F *et al* 1982 *Phys. Rev. Lett.* **49** 1408
[6] Jovanovic M R *et al* 2014 *Phys. Fluids* **26** 024103
[7] Taylor R *et al* 2018 *Rev. Sci. Instrum.* **89** 053501
[8] Hemati M S *et al* 2014 *Phys. Fluids* **26** 111701
[9] Kasuya N *et al* 2008 *Phys. Plasmas* **15** 052302
[10] Sasaki M *et al* 2017 *Phys. Plasmas* **24** 112103
[11] Inagaki S *et al* 2016 *Sci. Rep.* **6** 22189
[12] David P A *et al* 2016 *Phys. Plasmas* **23** 103511
[13] Sasaki M *et al* 2019 *Phys. Plasmas* **26** 042305
[14] Nishino N *et al* 2010 *J. Plasma Fusion Res.* **86** 648
[15] Ohdachi S *et al* 2003 *Rev. Sci. Instrum.* **74** 2136
[16] del-Castillo-Negrete D *et al* 2007 *J. Comp. Phys* **222** 265
[17] Beyer P *et al* 2000 *Phys. Rev. E* **61** 813
[18] Zweben S J *et al* 2002 *Phys. Plasmas* **9** 1981
[19] Maqueda R J *et al* 2003 *Rev. Sci. Instrum.* **74** 2020
[20] Myra J R *et al* 2018 *Plasma Phys. Control. Fusion* **60** 075015
[21] McKee G R *et al* 2004 *Rev. Sci. Instrum.* **75** 3490
[22] Fenzi C *et al* 2001 *Rev. Sci. Instrum.* **72** 988
[23] Iraji D *et al* 2010 *Phys. Plasmas* **17** 122304
[24] Fujisawa A *et al* 2016 *Plasma Phys. Control. Fusion* **58** 025005